Title	A mechanically reliable transparent antifogging coating on polymeric lenses
Author(s)	Ye Sun, Rajdeep Singh Rawat and Zhong Chen

A Mechanically Reliable Transparent Antifogging Coating on Polymeric Lenses

Ye Sun, Rajdeep Singh Rawat, Zhong Chen**

Ye Sun, Prof. Zhong Chen
School of Material Science and Engineering,
Nanyang Technological University,
Singapore 639798, Singapore
E-mail: ASZChen@ntu.edu.sg
Prof. Rajdeep Singh Rawat
Natural Science and Science Education,
National Institute of Education, Nanyang Technological University,
Singapore 637616, Singapore
E-mail: rajdeep.rawat@nie.edu.sg

* To whom correspondence should be addressed. E-mail: ASZChen@ntu.edu.sg (Z.C); rajdeep.rawat@nie.edu.sg (R.S.R)

Keywords: Superhydrophilic, Antifogging, Antireflection, Mechanical Robustness, Polymer lens

Abstract

Polymeric lenses have been increasingly used to replace glass lenses due to advantages of light weight, high refractive index, and ease of making into complicated shapes. However, a severe constraint to their wider application lies with their intrinsic weakness in hardness that can lead to mechanical damages by abrasion. During service, fogging remains another unsolved challenge to optical lenses, which may significantly reduce the users' visibility or even cause accident. Therefore, it is imperative to develop mechanically reliable and transparent antifogging coating on polymeric lenses. In the current work, we have developed a two-step protocol comprising a room temperature oxygen plasma treatment of polymer substrate followed by antifogging silica thin film deposition using pulsed laser deposition (PLD). The oxygen plasma treatment modifies the surface chemistry to allow a strong adhesion between the polymer substrate and the silica coating. Due to the porous nature of the PLD deposited nano-silica film, the coating also displays an antireflection effect. This mechanically reliable and highly transparent superhydrophilic silica coating opens great opportunity for the eyewear and high precision optics industries.

1. Introduction

Fogging occurs when water droplets, typically tens of micrometer in size, condense on a solid surface as the surrounding temperature suddenly falls below the dew point of the water-containing vapor [1]. Fogging causes light scattering and reduces optical transmission. A spectacle wearer often experiences severely reduced or even blocked vision when entering a warmer environment. Fogging may cause more serious consequences when it occurs on optical lenses of critical instruments [2], such as the ones in surveillance camera and autonomous vehicles. Extensive research has been carried out to prevent fog formation with limited success. Antifogging liquid sprays are commercially available for spectacles and other optical lenses; however, these sprays have to be re-applied frequently. Therefore, they are not suitable for many applications, particularly the ones in remote regions or under harsh working environment where maintenance is laborious and costly. Polymer-based antifogging coatings have been developed [3]; however, these organic coatings tend to be vulnerable to mechanical damages caused by abrasion and scratch. Inorganic coatings are mechanically more durable against these potential mechanical damages.

With the rapid advancement in processing technology and synthesis of new materials, high-quality polymeric optical lenses and screens have been increasingly utilized in defense, medical, biomedical, security, and consumer products [4]. Compared to the conventional inorganic materials such as glass, polymers enjoy the advantages of light weight, high resistance to impact damage, and easiness of making into complex shapes. On the other hand, polymeric surfaces are mechanically weak as they can be easily damaged by mechanical abrasion. Therefore, it is necessary to protect the polymer substrate by inorganic coatings while retaining their beneficial attributes of the bulk [5].

Based on the surface physics, organic surface has a lower surface energy and tends to "dislike" inorganic coatings that have a higher surface energy. It is therefore necessary to modify the polymer surface before the inorganic coating is applied to enhance the adhesion between the coating and the substrate.

Antifogging can be realized through constructing superhydrophilic surfaces [6] on which water droplets quickly coalesce and spread out evenly as a uniform liquid film. A number of techniques have been explored in the past, such as layer-by-layer deposition [7], dip-coating [8], and sol-gel coating [9]. Depending on the coating formulation, some coatings may require post-deposition curing by calcination [7b, 10] or UV irradiation [11]. Inorganic materials can resist the heating treatment of several hundred degrees; however, most polymeric materials are not able to sustain heating above 100°C. Therefore, it is highly desirable to develop a low-temperature coating process in our current study. Among various thin film deposition techniques, laser ablation deposition has been extensively used to construct nanostructured thin films [12] for various applications, including superconductors[13], protective coatings[14], and biocompatible coatings[15]. We used this technique in the current work as it allows good control of the film thickness and morphology. It also enables good quality film deposition without heating up the substrate, which is needed for heat sensitive materials like polymers.

In this work, we have developed a facile two-step method comprising of oxygen plasma surface treatment followed by deposition of nano porous silica film using pulse laser deposition (PLD) to obtain antifogging coating on polymer substrate (Polycarbonate, PC) at ambient temperature. The thin nano porous surface structure, coupled with specific surface chemical decoration, endows the coating with the superhydrophilicity,

high transparency, necessary mechanical reliability, antireflection, and excellent antifogging performance.

2. Results and Discussion

2.1 Surface Morphology and Light Transmission

Both surface roughness and surface chemistry have to be properly adjusted to control the wettability of a solid surface [16]. We first investigated the surface morphology of the as-prepared silica film by Field Emission Scanning Electron Microscope (FE-SEM) and Atomic Force Microscope (AFM, **Figure S1** of supporting information). As shown in **Figure 1A**, silica nanoparticles with an average size of about 41.9 ± 11.7 nm with small cluster in the size of 100 to 200 nm are uniformly distributed on surface without large aggregates. Surface topology and roughness were studied using AFM **(Figure 1B**). The prepared silica nanoparticle film exhibits a root-mean-square roughness (R_q) of 40.1 nm, which is higher than the pristine polycarbonate surface (Supporting Information, **Table S1**) with R_q value of 2.2 nm. Film thickness is 51 ± 2.8 nm based on the step profile in AFM measurement as shown in **Figure 1C**.

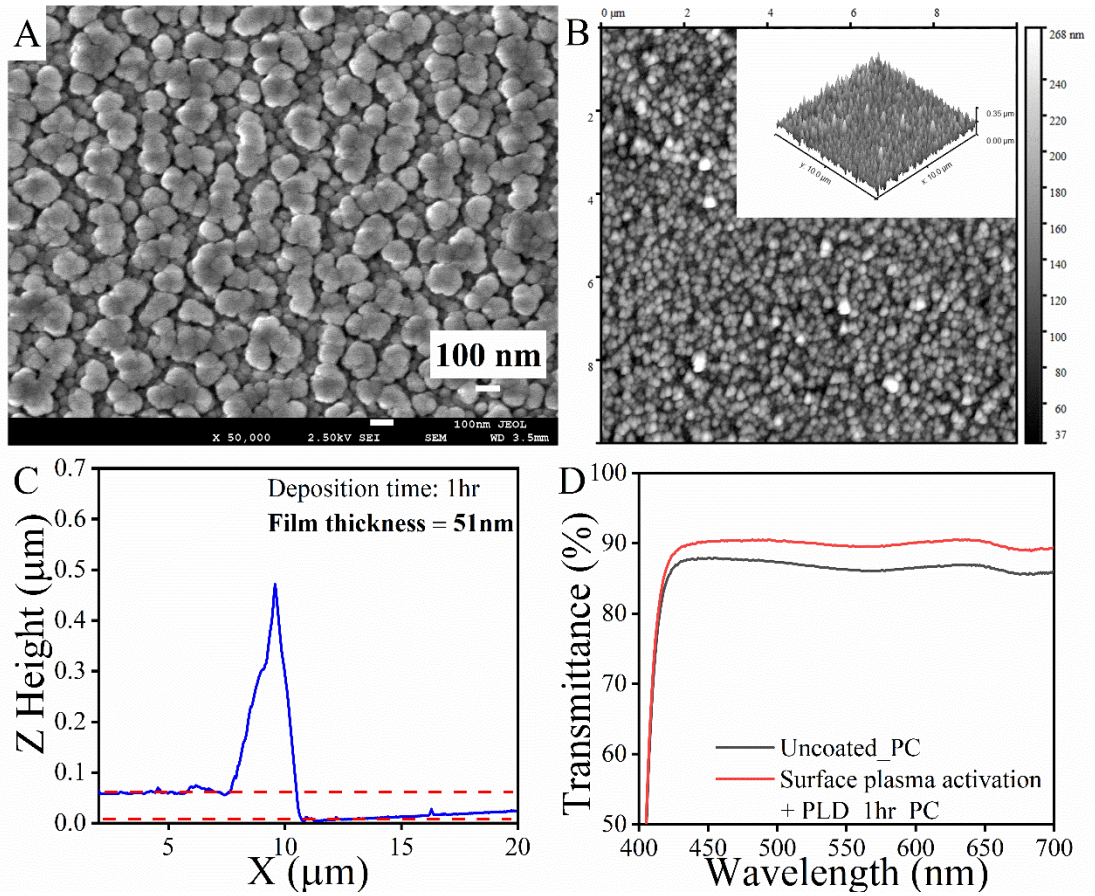

Figure 1. (A) Superhydrophilic silica nanoparticles film FE-SEM image; **(B)** AFM image of the nanoparticles film (10 µm × 10 µm), inset is a 3D image; **(C)** film thickness measured by AFM profile scan; **(D)** Transmission spectra of as-prepared superhydrophilic silica coating on PC.

The optical transmission was assessed by the light transmittance (T%) of uncoated and coated PC samples using UV-Vis spectroscopy. As shown in **Figure 1D**, the silica coated sample clearly has a higher transmittance in the visible range (420 nm to 700 nm) than the uncoated substrate at the incident angle of 0°. The average transmittance (T%) increases from 86.7% (without the coating) to 89.9% (with the coating). Despite the slightly increased surface roughness, the surface features are still much below the wavelength of visible light, thus light will not be scattered by the film. On the contrary,

the transmittance in the vertical direction has increased with the coating. The improved transmittance indicates antireflective characteristics of the coating, which can be explained as follows. Typically, in a single-layer antireflection film system, a lower refractive index coating material on substrate is desirable to obtain a high transmittance. For ideal antireflection in air-substrate interface, the refractive index of the coating is given by $n_{coat} = \sqrt{n_{air} \times n_{sub}}$ [17], where n_{air} and n_{sub} are the refractive index of air and substrate. Given that n_{air} and n_{sub} are 1.0 and 1.6 (for air and polycarbonate substrate), respectively, n_{coat} should be ideally around 1.26. This value is lower than most homogeneous dielectric materials, for example, the refractive index of silica is around 1.45 [18]. Hence, a dense silica coating is expected to have little or no antireflective effect. In our study, however, the silica film (**Figure 1A**) possesses a porous structure, which can be considered as a composite of silica and air with a reduced refractive index. This composite would lead to a considerably lower refractive index than the one of dense film [19]. Thus, by adjusting the porosity, it is possible to tune the reflectivity of the film to realize the required antireflection.

The Haze value remains largely unchanged after the coating was applied, indicating the coating itself does not cause light scattering (supporting information **Figure S2**, **Table S2**).

In addition, effect of thickness on the optical property was also studied by varying the deposition time from 10 min to 30 min and 1 hr. The corresponding thickness is 7.1 ± 2.3 nm, 15 ± 3.1 nm, and 51 ± 2.8nm. Highest light transmittance was observed in the 30 min deposition sample. With further increase of the deposition time, slight drop of light transmittance was observed as shown in **Figure S3** (Supporting Information) due

to increased light absorbance in thicker films. On the other hand, a thicker film (1 hr deposition) provides better abrasion resistance, which will be discussed in the following section. Based on the overall performance, we choose 51 nm thick film for further evaluation unless otherwise indicated.

2.2 Wettability of the Superhydrophilic Silica Coating

Wettability of the coatings is characterized by water contact angle (WCA) measurements. Digital image and video recording of water-surface interaction were captured to examine the wetting behavior. As shown in **Figure 2A**, the WCA was reduced from 68.3 ± 4° to complete wetting (WCA ≈ 0°) after surface oxygen plasma treatment. The same complete wetting was also observed after the deposition of the silica nanoparticle film. Although complete wetting was observed after surface oxygen plasma treatment alone (shown in **Figure 2B**), "hydrophobic recovery" [20] was observed after a few days of exposure to atmospheric conditions, due to absorption of hydrophobic molecules in the atmosphere or reorientation of surface functional groups between surface and bulk through diffusion. This implies that the oxygen plasma treated surface has slowly returned to its original state before the treatment. On the other hand, silica film deposited on PC after the oxygen plasma treatment was significantly stable. It has maintained its excellent hydrophilicity even after more than 100 days of exposure to ambient conditions. In addition, the coating was exposed to high-temperature vapor to examine the durability again hot steam. The superhydrophilicity remained after 10 hr exposure as shown in **Figure 2C**.

The water droplet spreads on the coated surface quickly. **Figure 2D** and **E** display the digital images taken at 0 and 93 ms, respectively, after the water droplet was placed on the surface. Within 100 ms, the water droplet has fully spread over the surface, which confirms the excellent wettability of the coating. The interaction of water droplets with coated surface was also recorded by high-speed camera (**Supporting Information - Video**).

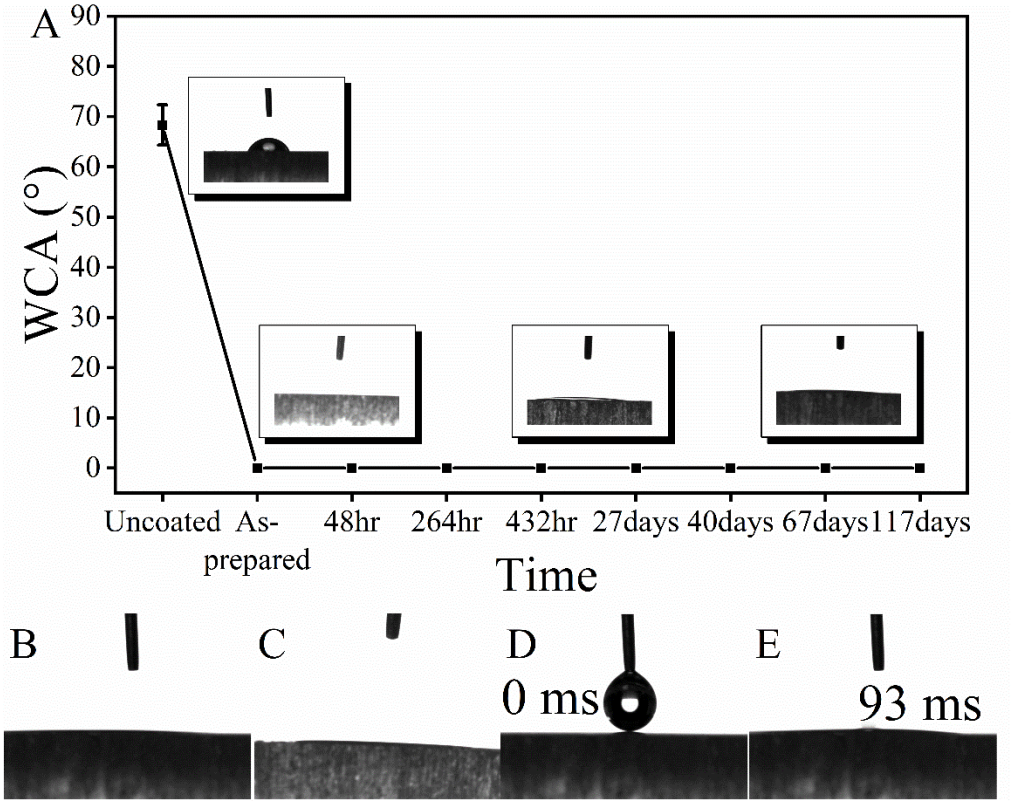

Figure 2. WCA of the superhydrophilic silica film; **(A)** WCA measurement over time, up to 117 days; **(B)** WCA ≈ 0° after oxygen plasma treatment; **(C)** WCA measurement of coated sample after exposure to high-temperature steam for 10 hr; **(D)** and **(E)** show the fast-spreading behaviour of water on silica coating within 100 ms.

2.3 Antifogging Performance

Figure 3 shows the fogging test results using two widely recognized testing methods for PC substrate materials. In the steam test as shown in **Figure 3A** and **B**, the uncoated PC lens fogged immediately upon exposure to water steam, whereas the superhydrophilic silica surface remained transparent. Fridge test was also performed by placing uncoated and coated PC inside a fridge set at -6°C for 24 hr [21] and then exposed to laboratory environment (room temperature 21-25°C, RH: 50-60%). As shown in **Figure 3C**, the silica coated PC surface remained fog-free while the uncoated PC samples were fogged. Therefore, this developed superhydrophilic silica nanoparticles film can effectively prevent the formation of fog due to the strong affinity to water.

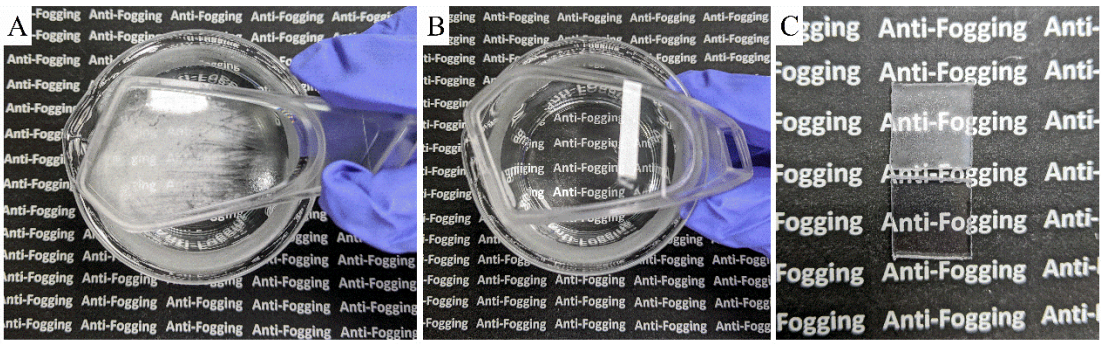

Figure 3. Digital image exhibiting the antifogging property of coated and uncoated polycarbonate substrate. **(A)** uncoated PC substrate and **(B)** silica coated PC substrate undergo steam test; **(C)** comparison of uncoated (top) and coated (bottom) PC substrate taken from refrigerator at -6°C to laboratory environment.

We have also deposited the same superhydrophilic silica films on another polymer substrate, Zeonex® E48R, which is commercially used for optics and eyewear due to its excellent optical properties including high transparency and low water absorption.

Excellent antireflection (average transmittance increases from 91.7% to 94%) and antifogging performances were observed (**Figure S4**, Supporting Information).

2.4 Surface Chemistry Analysis

The excellent antifogging performance and good stability of the as-prepared superhydrophilic silica film can be expounded by surface X-ray photoelectron spectroscopy (XPS). **Figure 4A** shows the comparison of XPS survey spectra of untreated, oxygen plasma treated, the as-prepared silica nanoparticle film, and lastly the silica film after being exposed to ambient environment for 117 days. The elemental composition of PC with and without the coating is summarized in **Table 1**. A significant increament of surface oxygen peak after the oxygen plasma treatment was observed. The high-resolution fitted XPS spectra of C 1s between untreated and oxygen plasma treated samples (Figure **4B** and **C**) indicates that extra oxygen bond C=O (288.8 eV) and COOR (290.7 eV) appeared after the plasma treatment. Abundant oxygen bonding on the surface created by oxygen plasma treatment helps increase the surface energy of the substrate from 28.0 to 74.8 mJ/m^2 (**Table S1**, Supporting Information), which could enhance the adhesion with the subsequently deposited silica film. Survey spectra of the as-prepared silica nanoparticle film in Figure **4A** indicate that the surface coating consists of carbon (C), oxygen (O), and silicon (Si). The significant reduction of C peak is due to the silica nanoparticle film on the substrate surface. The O 1s peak at 532.7 eV and the Si 2p peak at 103.3 eV in high-resolution spectra (**Figure 4D** and **E**) of the silica film are characterized as Si-O-Si bond. In addition, the broadened peak centred around $2\theta = 23°$ in the X-ray diffraction (XRD) pattern in **Figure 4G** suggests that the silica film was amorphous [22]. It is well documented [23] that the surface of silica is

intrinsically hydrophilic as it is covered with silanol group (Si-OH). Silanol groups have strong affinity with water through the formation of hydrogen bonds. The hydroxyl group (-OH) on silica film was identified by fourier transform infra-red spectroscopy (FTIR) as indicated in **Figure 4F** in the range of 3000 cm^{-1} to 3800 cm^{-1}. The density of hydroxyle group was measured to be 2.46 ± 0.01 nm^{-2} as detailed in the supporting information (**Figure S5**, **Table S3**).

Due to the specific surface morphology and chemical composition, the as-prepared silica nanoparticle film exhibits excellent hydrophilicity and antifogging performance. The abundant silanol groups on the surface favors H-bonding with water, while the

nanopores formed during film deposition facilitates water spreading by wicking effect [24]. The reduced film refractive index contributes to the antireflectivity of the coating.

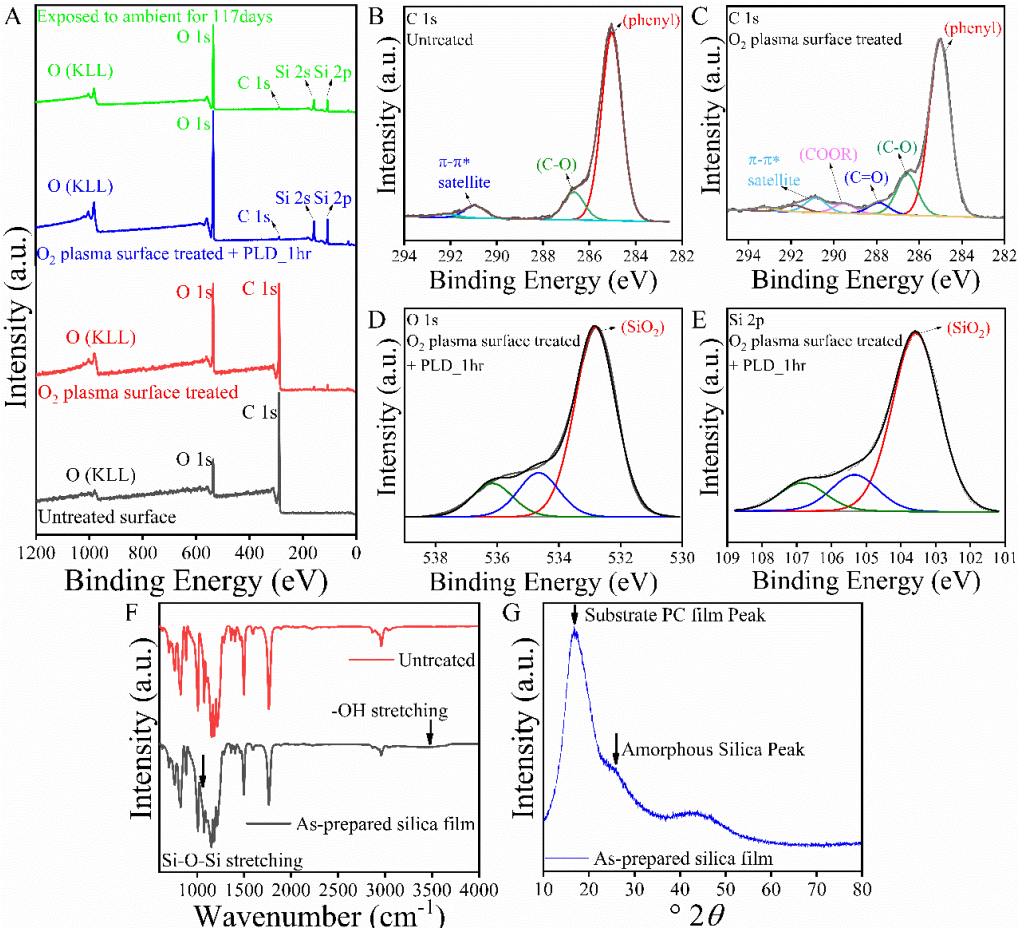

Figure 4. XPS spectra of the superhydrophilic silica nanoparticle coating on polycarbonate substrate **(A)** Survey XPS spectra comparison between untreated, oxygen plasma surface treated, as-prepared superhydrophilic silica nanoparticle film and after exposed to ambient condition for 117days; **(B)** and **(C)** are high resolution fitted XPS spectra of C 1s of untreated and oxygen plasma treated surface; **(D)** and **(E)** are high resolution fitted XPS spectra of O 1s and Si 2p of as-prepared silica nanoparticle film; **(F)** FTIR spectra of pristine PC surface as well as superhydrophilic silica coated PC surface; **(G)** XRD pattern spectra.

Table 1. Atomic concentration of elements using XPS

Pristine PC		Superhydrophilic silica nanoparticles film coated PC		
Atomic Concentration of Elements %				
C	**O**	**C**	**O**	**Si**
89.19	**10.48**	**5.11**	**62.79**	**32.11**

2.5 Mechanical Robustness and Durability

Mechanical robustness and durability are the main considerations for practical applications of superhydrophilic coatings. In this study, we evaluate the coating's mechanical robustness by examining the coating adhesion as well as the abrasion resistance based on the MIL-C-48497 standard. This particular standard is the most appropriate specification for optical coating [25]. In the first examination, as shown in **Figure 5A** and **B**, observation by naked eyes did not find any significant coating damage after the adhesion test. To further evaluate the adhesion strength and the film quality, crosshatch test based on ASTM D3359 standard was performed. **Figure 5C** shows no coating chipping along the crosshatched lines, indicating a "clean" cut.

In addition, coating durability was evaluated by a surface abrasion test using a cheese cloth, which is part of the MIL-C-48407 tests. Surface morphology was partially changed by the abrasion as observed in **Figure 5D**, due to the small amount of residues from the abrasion cloth. Surface roughness (R_q) slightly decreased to around 20 nm. However, good wettability (WCA ≈ 4°) was still observed after the abrasion test. **Figures 5E** and **5F** show that the surface after the abrasion and adhesion test still possess good water wettability and antifogging performance by the 1 hr depostion

sample. While for coating deposited for 10 min and 30 min, superhydrophilicity was partically lost after abrasion test as indicated in **Figure S7A** and **B** (Supporting Information). Therefore, we recommend 1 hr deposition because of the better mechanical robustness with minimum compromise in the optical transmittance. Cross sectional SEM image using Focus Ion Beam (FIB) also indicates the good adhesion between the nanoparticles and substrate without observing any void at the interface in the 51 nm film (**Figure S6**, Supporting Information). Light transmission afte tape and abrasion test was also performed. Surface after the abrasion and tape test retains its antireflection property despite a slight drop of light transmittance (from 89.9% to 88.7%) as indicated in **Figure S7** (Supporting Information). This again, is likely due to the cloth residues as explained before.

Silica coatings prepared on PC substrate without going through the oxygen plasma treatment were also examined for comparison. Surface morphology observed under FESEM shows a smaller silica particle size (**Figure 5H**). It is known that surface energy affects the surface nucleation [26]. The higher the surface energy, the lower the nucleation barrier. Therefore, PC substrate that has undergone oxygen plasma treatment should possess a higher surface energy than the untreated PC surface (**Table S1**, Supporting Information) that promotes the nucleation and growth of the oxide particles. On the other hand, surface without oxygen plasma activation has a lower surface energy. The adsorption energy of an atom on the substrate is much larger than on the growing film. Thus, a smaller particle growth can be observed. Although naked eye observation was not able to identify the coating damage, SEM images in **Figure 5H** and **5I** clearly show delamination of coating after the tape adhesion test. The comparision indicates

that oxygen plasma treatment of the PC substrate is critical to the enhancement of film adhesion to the substrate.

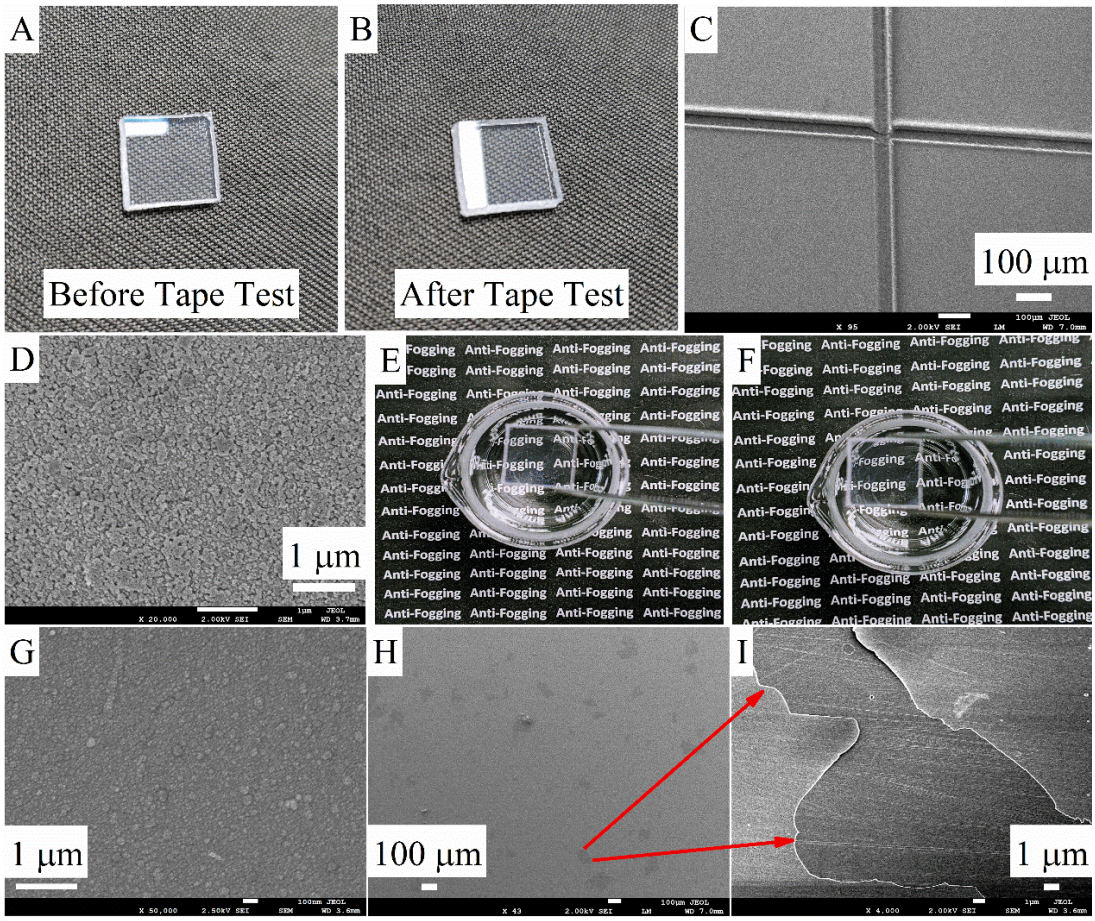

Figure 5. Mechanical and durability tests of as-prepared silica nanoparticle films on PC substrate; Surface before **(A)** and after **(B)** tape test; **(C)** SEM observation of crosshatch film; **(D)** SEM observation of sample that undergoes abrasion test; **(E)** and **(F)** steam testing for antifogging performance after the tape test and abrasion test; **(G)** surface morphology of the film deposited on PC substrate without plasma treatment; **(H)** and **(I)** coating delamination of film deposited without plasma treatment after tape test.

3. Conclusion

We have reported a facile, two-step room temperature process for deposition of superhydrophilic silica coating on polymeric optical substrates. The coated films are composed of porous amorphous silica nanoparticles. The combination of surface with hydrophilic silanol groups and nanoporous topography endows the prepared silica nanoparticle film with excellent antifogging and antireflection performances. The silica-based coatings prove to be mechanically robust and durable, making it one step closer to practical applications in the eyewear and polymer optics industry.

4. Experimental Section

Coating of silica nanoparticles film

The superhydrophilic silica coatings on polymeric substates were prepared via a two-step process. First, polymer lens material, polycarbonate (PC) (1.5 cm × 1.5 cm) surface was cleaned with ethanol and deionized water for several cycles, before being dried at 50°C. The sample was then placed inside a radio frequency (RF) plasma reactor chamber made of a quartz tube with two capacitively coupled ring electrodes mounted externally on the quartz tube. The quartz tube was evacuated to base pressure below 10^{-3} mbar. Oxygen gas was then introduced into the reactor chamber at a flow rate of 2 sccm, under which the chamber pressure was stabilized at 10^{-2} mbar. Oxygen plasma was then generated with 250 W RF power using a 13.56 MHz Caeser136 RF generator connected to the ring electrode through auto-impedance matching unit. The oxygen plasma treatment of PC was carried out for 10 min. In the second step, the oxygen plasma treated substrate was placed in a pulse laser deposition (PLD) chamber. Silicon target (purchased from S1-Lab Pte Ltd, 99.99%) was placed at 5 cm away from the substrate. Nd:YAG 532 nm laser was operated at 10 Hz with laser pulse fluence of $F = 4.74\ \mathrm{Jcm^{-2}}$. The laser beam is focused to a spot size ≈ 5.0×10^{-4} cm^2 on silicon target surface. The PLD chamber was pumped down to 10^{-5} mbar. Oxygen was introduced into the chamber at the start of deposition at a flow rate of 200 sccm. The PLD chamber pressure was stabilized at 10^{-2} mbar. The deposition was carried out for 10 min, 30 min, and 1 hr at 10 Hz laser operating frequency. The schematic of fabrication process as shown in **Figure 6**.

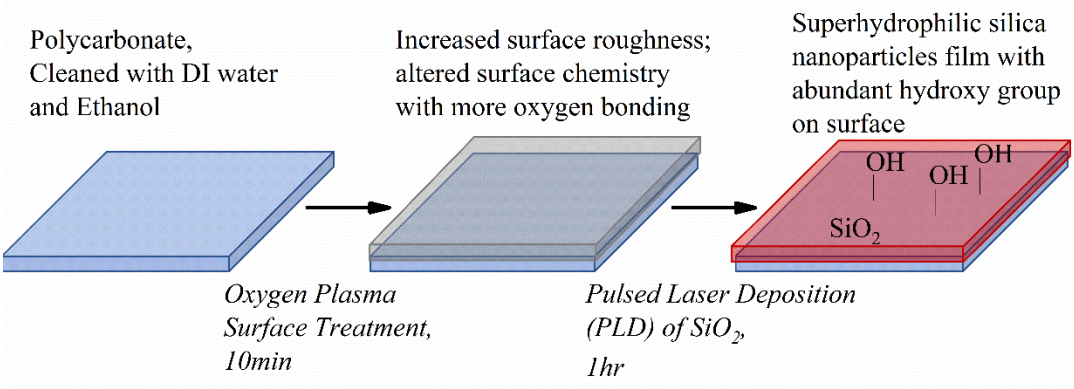

Figure 6. Schematic fabrication process of superhydrophilic silica nanoparticles film coating on PC.

Material Characterization

The surface morphology was observed using a JEOL 7600 field emission scanning microscope (FESEM) operated at 2.5 kV. A NX10 Park system atomic force microscope (AFM) was used to examine the surface topology. A Perkin Elmer Frontier Fourier Transformation Infra-Red (FTIR) spectrometer was used to understand chemical molecular bonding. Kratos AXIS Supra X-ray Photoelectron Spectrometer (XPS) was applied for the surface chemical composition analysis. The binding energy of the C 1s peak from sp2-bonded carbon at 284.8 eV was used as a reference. Water contact angle (WCA) was recorded using a contact angle goniometer (OCA 20 Dataphysics) with 5µL DI water droplet. The surface energy was calculated using the OWRK method [27] using three different liquids: DI water, glycerol, and ethylene glycol. Transmittance was measured by Perkin Elmer Lambda 950 UV-Vis-NIR spectrometer.

Mechanical Durability testing based on MIL-C-48497 and ASTM 3359

Moderate Abrasion resistance test was done based on MIL-C-48497 test standard. Abrasion action was carried out with rubbing of the surface using a cheese cloth pad at a constant force (400-gram weight uniformly distributed onto 1.5 cm × 1.5 cm substrates, the corresponding pressure is 26.7 kPa). 20 strokes of rubbing action in total was carried out.

Adhesion was examined based on MIL-C-48497. A cellophane tape was pressed in contact with surface coating and then pulled off slowly at an angle of 45°.

Crosshatch adhesion test was conducted based on ASTM D3359 standard. The surface coating was crosscut with a harden steel cutter. Cellophane tape was then applied on surface and then pulled off slowly.

Durability again high-temperature vapor was carried out by placing the coated samples over a hot water steam for up to 10 hr. Water contact angle was measured after the exposure to examine the wettability.

Acknowledgements

The authors thank the technical support from Facility for Analysis Characterization Testing & Simulation (F.A.C.T) in Nanyang Technological University. Sample preparation using FIB was carried out by Dr. Xun Cao. This work was financially supported by Ministry of Education, Singapore (RG16/18, RG8/21) and NIE RS-SAA grant no. RS 6/18 RSR.

Conflict of Interest

The authors declare no conflict of interest.

We have successfully developed a room temperature facile process that modifies the surface of polymeric materials to endow it with excellent antifogging and antireflection properties. The as-prepared coating is mechanically robust and durable, making it one step closer to practical applications in the eyewear and polymer optics industry.

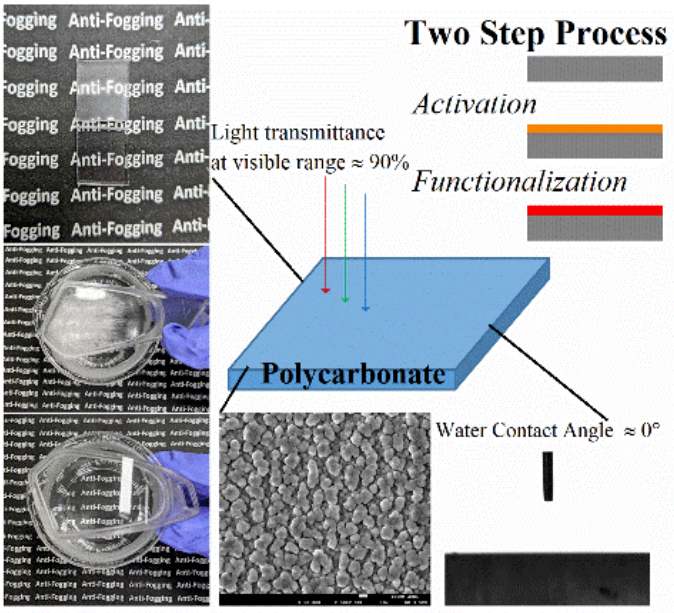

Reference

[1] Z. Zheng, Y. Liu, L. Wang, L. Yu, Y. Cen, T. Zhu, D. Yu, C. Chen, *Progress in Organic Coatings* **2020**, 142, 105578.

[2] K. Oguri, N. Iwataka, A. Tonegawa, Y. Hirose, K. Takayama, Y. Nishi, *Journal of Materials Research* **2001**, 16, 553.

[3] a) J. Zhao, L. Ma, W. Millians, T. Wu, W. Ming, *ACS Applied Materials & Interfaces* **2016**, 8, 8737; b) K. Manabe, C. Tanaka, Y. Moriyama, M. Tenjimbayashi, C. Nakamura, Y. Tokura, T. Matsubayashi, K.-H. Kyung, S. Shiratori, *ACS Applied Materials & Interfaces* **2016**, 8, 31951.

[4] W. Beich, *Injection molded polymer optics in the 21st-Century*, SPIE, **2005**.

[5] a) Z. Chen, L. Y. L. Wu, E. Chwa, O. Tham, *Materials Science and Engineering: A* **2008**, 493, 292; b) L. Y. L. Wu, E. Chwa, Z. Chen, X. T. Zeng, *Thin Solid Films* **2008**, 516, 1056.

[6] a) J. Drelich, E. Chibowski, *Langmuir* **2010**, 26, 18621; b) M. Florea-Spiroiu, D. Achimescu, I. Stanculescu, M. Purica, R. Gavrila, S. Peretz, *Polymer Bulletin* **2013**, 70, 3305; c) X. Zhang, J. He, *International Journal of Nanoscience* **2014**, 14, 1460015.

[7] a) X. Li, X. Du, J. He, *Langmuir* **2010**, 26, 13528; b) Q. Shang, Y. Zhou, *Ceramics International* **2016**, 42, 8706; c) J. Zhang, L. Jiang, W. Zhao, Z. Yang, H. Nie, Z. Yao, *Polymer Testing* **2019**, 77, 105907; d) X. Liu, X. Du, J. He, *ChemPhysChem* **2008**, 9, 305.

[8] a) X. Du, Y. Xing, M. Zhou, X. Li, H. Huang, X.-M. Meng, Y. Wen, X. Zhang, *Microporous and Mesoporous Materials* **2018**, 255, 84; b) T. Zhang, L. Fang, N. Lin, J. Wang, Y. Wang, T. Wu, P. Song, *Green Chemistry* **2019**, 21, 5405; c) X. Li, B. Shi, W. Chaikittisilp, M. Li, Y. Wang, Y. Liu, L. Gao, L. Mao, *Journal of Materials Science* **2016**, 51, 6192.

[9] a) X. Du, X. Liu, H. Chen, J. He, *The Journal of Physical Chemistry C* **2009**, 113, 9063; b) L. Ye, Y. Zhang, C. Song, Y. Li, B. Jiang, *Materials Letters* **2017**, 188, 316; c) D. Wang, Y. Li, Y. Wen, X. Li, X. Du, *Colloids and Surfaces A: Physicochemical and Engineering Aspects* **2021**, 629, 127522.

[10] L. Xu, J. He, L. Yao, *Journal of Materials Chemistry A* **2014**, 2, 402.

[11] Y. Chen, C. Zhang, W. Huang, C. Yang, T. Huang, Y. Situ, H. Huang, *Surface and Coatings Technology* **2014**, 258, 531.

[12] C. W. Schneider, T. Lippert, in *Laser Processing of Materials: Fundamentals, Applications and Developments*, DOI: 10.1007/978-3-642-13281-0_5 (Ed: P. Schaaf), Springer Berlin Heidelberg, Berlin, Heidelberg **2010**, p. 89.

[13] D. Xu, Y. Wang, L. Liu, Y. Li, *Thin Solid Films* **2013**, 529, 10.

[14] M. Kalin, M. Polajnar, *Applied Surface Science* **2014**, 293, 97.

[15] F. Sima, C. Ristoscu, L. Duta, O. Gallet, K. Anselme, I. N. Mihailescu, in *Laser Surface Modification of Biomaterials*, DOI: https://doi.org/10.1016/B978-0-08-100883-6.00003-4 (Ed: R. Vilar), Woodhead Publishing **2016**, p. 77.

[16] I. R. Durán, G. Laroche, *Progress in Materials Science* **2019**, 99, 106.

[17] H. K. Raut, V. A. Ganesh, A. S. Nair, S. Ramakrishna, *Energy & Environmental Science* **2011**, 4, 3779.

[18] I. H. Malitson, *J. Opt. Soc. Am.* **1965**, 55, 1205.

[19] W. Shimizu, Y. Murakami, *ACS Applied Materials & Interfaces* **2010**, 2, 3128.

[20] R. Di Mundo, R. d'Agostino, F. Palumbo, *ACS Appl Mater Interfaces* **2014**, 6, 17059.

[21] X. Zhang, J. He, *International Journal of Nanoscience* **2015**, 14, 1460015.

[22] M. Waseem, S. Mustafa, A. Naeem, K. Shah, I. Shah, H. Ihsan Ul, *J. Pak. Mater. Soc.* **2009**, 3, 19.
[23] L. T. Zhuravlev, *Reaction Kinetics and Catalysis Letters* **1993**, 50, 15.
[24] A. Girard, M. Amaya, H. Wi, *Journal of Heat Transfer* **2015**, 137.
[25] D. Sanchez, Vol. 17, CERAC Coating Materials News 2007.
[26] N. T. K. Thanh, N. Maclean, S. Mahiddine, *Chemical Reviews* **2014**, 114, 7610.
[27] D. K. Owens, R. C. Wendt, *Journal of Applied Polymer Science* **1969**, 13, 1741.

Supporting Information

A Mechanically Reliable Transparent Antifogging Coating on Polymeric Lenses

Ye Sun, Rajdeep Singh Rawat, Zhong Chen**

Ye Sun, Prof. Zhong Chen
School of Material Science and Engineering,
Nanyang Technological University,
Singapore 639798, Singapore
E-mail: ASZChen@ntu.edu.sg
Prof. Rajdeep Singh Rawat
Natural Science and Science Education,
National Institute of Education, Nanyang Technological University,
Singapore 637616, Singapore
E-mail: rajdeep.rawat@nie.edu.sg

* To whom correspondence should be addressed. E-mail: ASZChen@ntu.edu.sg (Z.C); rajdeep.rawat@nie.edu.sg (R.S.R)

Keywords: Superhydrophilic, Antifogging, Antireflection, Mechanically Robust, Polymer lens

Surface Topography and Its Effect on Wetting

Surface topography plays a crucial role in liquid spreading on a solid surface. In our work, **Figure S1** shows the topography of different surfaces: pristine PC, oxygen plasma treated PC, silica film deposited on oxygen plasma treated PC, and silica film deposited on pristine PC. Distinct differences were observed after oxygen plasma treatment as well as after deposition of silica film on oxygen plasma treated PC. Surface root-mean-square roughness (R_q) increased almost 20 times after oxygen plasma treatment and deposition of silica film on oxygen plasma treated PC as indicated in **Table S1**. Surface roughness factor (r), defined as the ratio of the true solid surface area over its horizontal projection, was calculated from the AFM measurement [1]. Based on the Wenzel theory [2], it is possible to achieve superhydrophilic surfaces by manipulating the surface roughness factor of a hydrophilic surface. In our study, oxygen plasma surface treatment has led to a surface roughness factor of 1.319. Following the Wenzel equation, then the apparent contact angle θ_{rough} can be described by:

$\cos\theta_{rough} = r \times \cos\theta$, [2]

where θ is the true contact angle on a flat surface and *r* is the surface roughness factor.

Based on the measured θ_{rough} and *r* values, we can calculate the "true" contact angle on a flat surface, and then calculate the true surface energy using the OWRK method. The apparent surface energy, calculated using the as-measured liquid contact angle, and the true surface energy, calculated using the flat surface contact angles, are displayed in **Table S1**. The surface energy, reflected through the contact angle measurement, is clearly "amplified" by a rough surface [3].

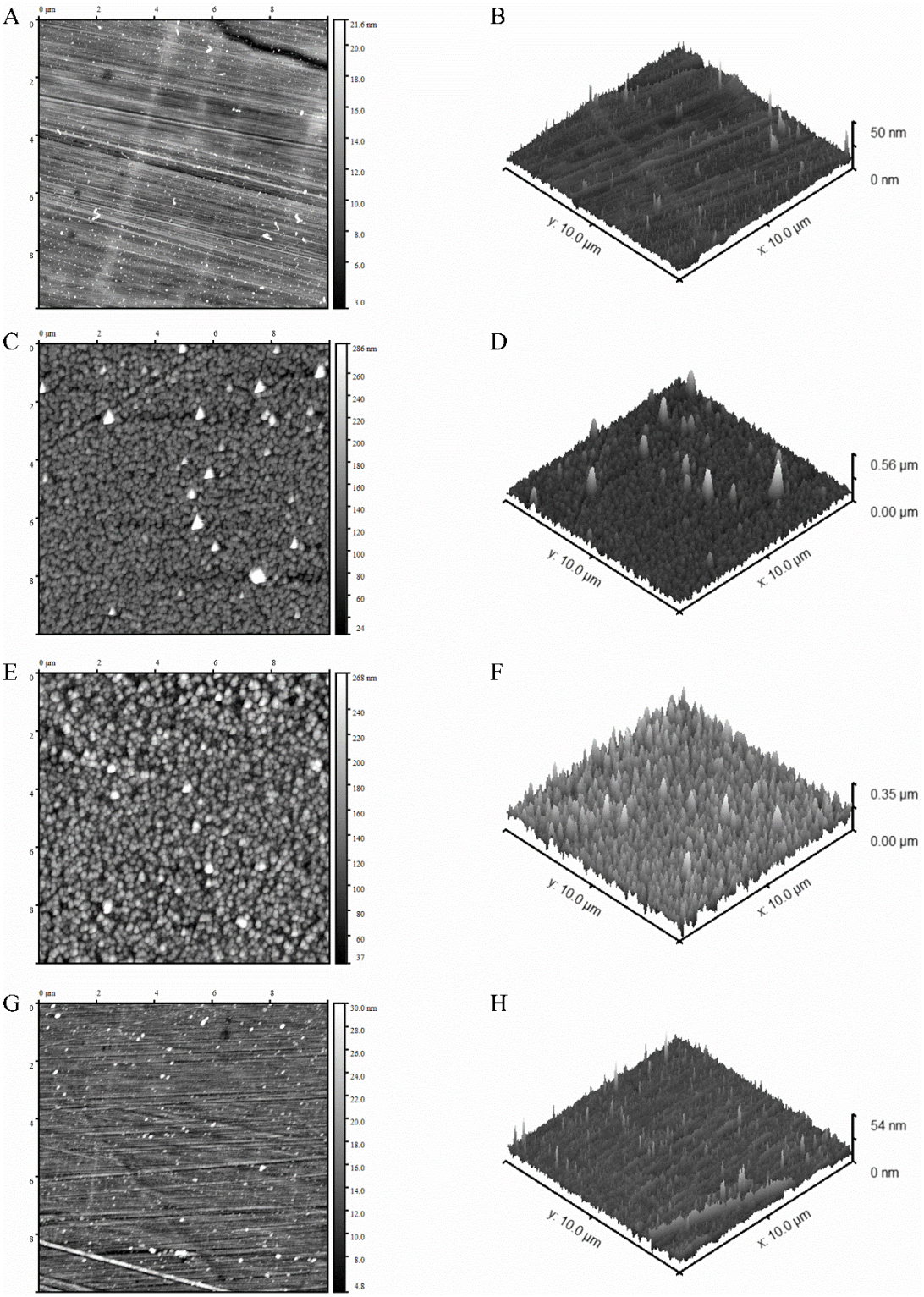

Figure S1. Surface morphology characterization by AFM; **(A)** and **(B)** pristine PC surface; **(C)** and **(D)** oxygen plasma treated PC surface; **(E)** and **(F)** silica film deposited on oxygen plasma treated PC; **(G)** and **(H)** silica film deposited on raw PC.

Table S1. Surface Free Energy Measurement, root-mean-square roughness R_q and surface roughness factor, r.

Substrate Condition	Apparent Surface Free Energy (mJ/m^2)	True Surface Free Energy (mJ/m^2)	Root-mean-square roughness, R_q (nm)	*r*, Roughness Factor
Raw PC	28.1	28.0	2.2	1.004
O_2 Plasma Treated PC	96.9	74.8	37.3	1.319
Silica Nanoparticle coating on O_2 Plasma Treated PC	99.0	76.1	40.1	1.322

Haze Measurement

Haze measurement was conducted according to ASTM-D-1003 test standard. Three different light transmittance was measurement in UV-Vis spectroscopy using an integrating sphere. Total light transmittance (T_t), sample diffusion rate (T_4), and instrument diffusion rate (T_3) were obtained as shown in **Figure S2**. Haze value was then calculated using these spectra as indicated in **Table S2**. Similar value of Haze measurement was observed between pristine PC and as-prepared silica coated PC.

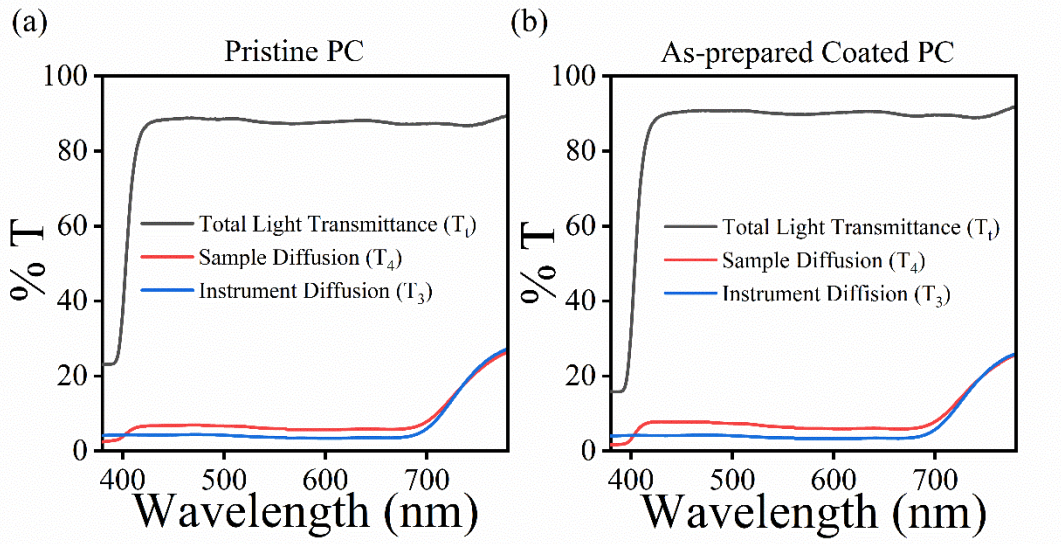

Figure S2. Transmittance spectra of Haze measurement.

Table S2. Calculated Haze value for pristine PC and as-prepared silica coated PC.

	Tt (%)	**T4 (%)**	**T3(%)**	**Haze (%)**
Pristine PC	87.64	5.62	3.2	3.15
As-prepared Coated PC	90.07	5.98	3.17	3.5

Film Thickness vs. Optical Transmittance

Effect of film thickness on optical transmittance was studied by varying different deposition duration. Thickness at 10 min, 30 min and 1 hr deposition duration is 7.1 ± 2.3 nm, 15 ± 3.1 nm, and 51 ± 2.8nm, respectively. Highest light transmittance at 30min of deposition was observed. With the increase of deposition time, slight drop of light transmittance can be observed as indicated in **Figure S3** due to light absorbance in thicker film.

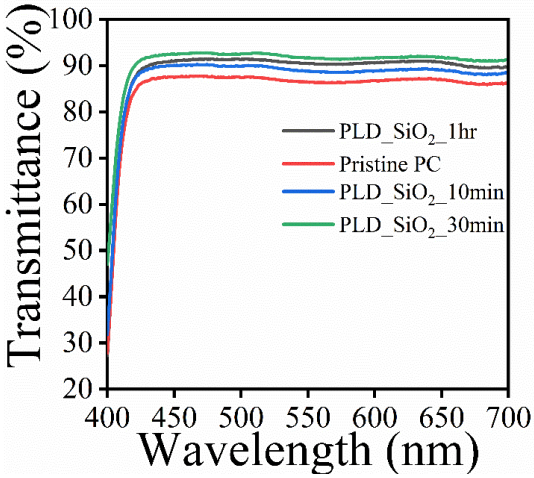

Figure S3. Light Transmittance with respect to different deposition duration.

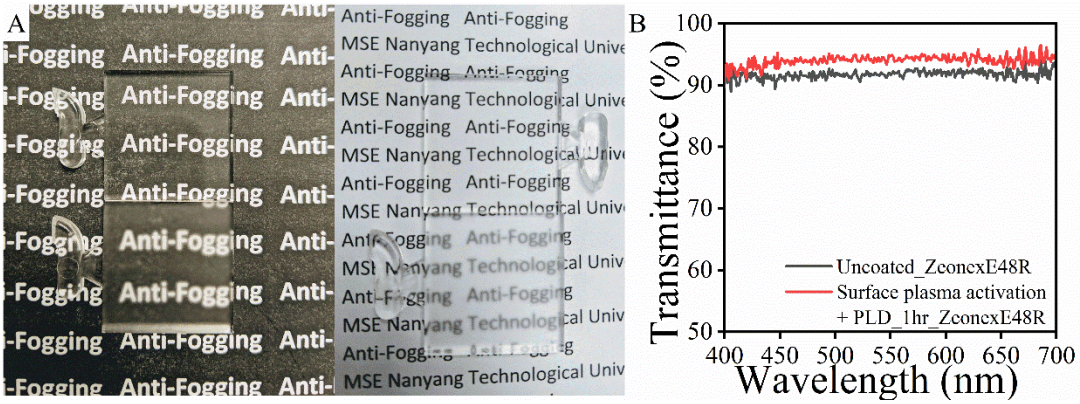

Figure S4. Antifogging and antireflection performance on ZeonexE48R® polymer substrate coated with the superhydrophilic silica.

Hydroxyl Group Density Measurement

The density of hydroxyl groups was quantified by measuring the contact angle with water of different pH value in octane following Liu et al. [4]. The maximum contact angle appeared at point of zero charge (**Figure S5**) was used to calculate the density of the hydroxyl groups on the superhydrophilic silica coated PC. As indicated in **Table S3**, the density of hydroxyl groups is 2.46 ± 0.01 OH nm^{-2}. For a completely hydroxylated silica surface, the average number is 4.9 OH nm^{-2}. This indicates that percentage coverage of hydroxyl groups on our as-prepared silica surface is around 50%.

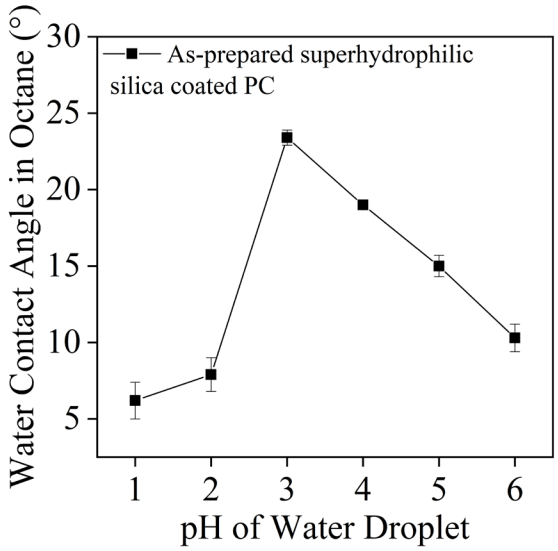

Figure S5. Water contact angle in Octane with reference to different water pH value

Table S3. The maximum contact angle corresponding to the point of zero charge and the density f hydroxyl groups calculated on as-prepared silica coated PC.

	θ_{Max} (°)	pzc	n_{OH}(nm^{-2})
Superhydrophilic silica coating (51 nm thick) on PC	23.4 ± 0.5	2.0	2.46 ± 0.01

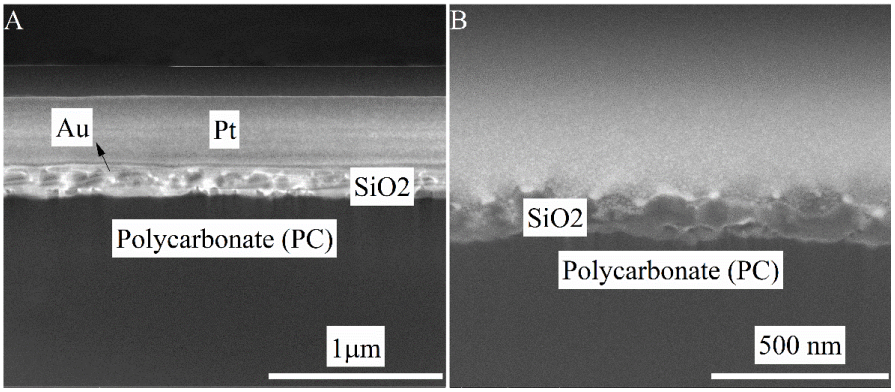

Figure S6. Cross section image of as-prepared silica nanoparticle film (51 nm thick) prepared by Focus Ion Beam (FIB); (A) SEM image and (B) back scattered SEM image.

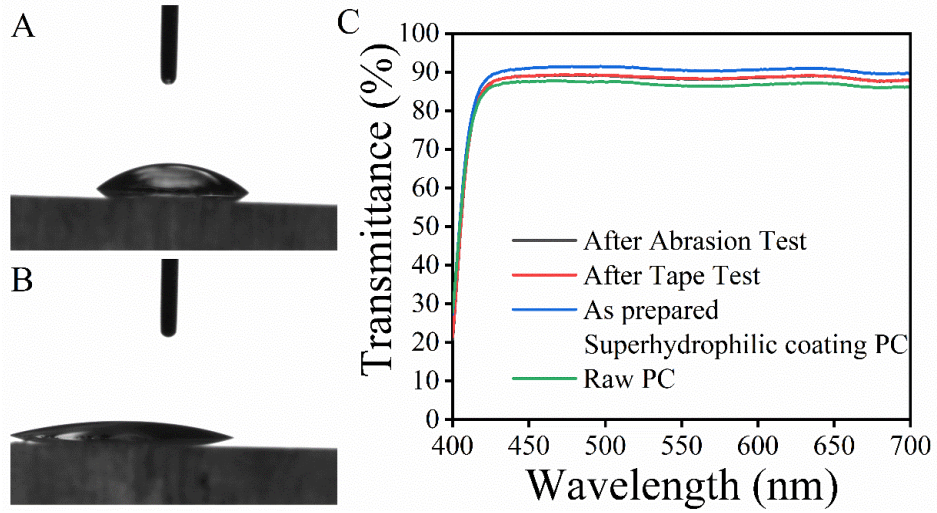

Figure S7. WCA measurement after abrasion test for samples deposited at (A) 10 min (B) 30 min; (C) Transmission spectra comparison of raw PC, as-prepared superhydrophilic silica coating (1 hr deposition) on PC, and the same silica coating after abrasion test and after tape peel test.

Supporting Information – Video (attached video file)

Reference

[1] L. Blunt, X. Jiang, in *Advanced Techniques for Assessment Surface Topography*, DOI: https://doi.org/10.1016/B978-190399611-9/50002-5 (Eds: L. Blunt, X. Jiang), Kogan Page Science, Oxford **2003**, p. 17.
[2] R. N. Wenzel, *Industrial & Engineering Chemistry* **1936**, 28, 988.
[3] G. McHale, N. J. Shirtcliffe, M. I. Newton, *Analyst* **2004**, 129, 284.
[4] X. M. Liu, J. Thomason, F. R. Jones, in *Silanes and Other Coupling Agents* Vol. 5, Brill Academic Publishers **2007**.